

Million-scale Object Detection with Large Vision Model

Feng Lin^{1,2}, Wenze Hu¹, Yaowei Wang³, Yonghong Tian³, Guangming Lu², Fanglin Chen², Yong Xu⁴ and Xiaoyu Wang^{1*}

¹Intellifusion Inc., Shenzhen, China .

²Harbin Institute of Technology, Shenzhen, China .

³Peng Cheng Laboratory, Shenzhen, China .

⁴South China University of Technology, Guangzhou, China.

*Corresponding author(s). E-mail(s): fanghuaxue@gmail.com;

Contributing authors: lin1993@mail.ustc.edu.cn; windsor.hwu@gmail.com;
wangyw@pcl.ac.cn; yhtian@pku.edu.cn; luguangm@hit.edu.cn; chenfanglin@hit.edu.cn;
yxu@scut.edu.cn;

Abstract

Over the past few years, developing a broad, universal, and general-purpose computer vision system has become a hot topic. A powerful universal system would be capable of solving diverse vision tasks simultaneously without being restricted to a specific problem or a specific data domain, which is of great importance in practical real-world computer vision applications. This study pushes the direction forward by concentrating on the million-scale multi-domain universal object detection problem. The problem is not trivial due to its complicated nature in terms of cross-dataset category label duplication, label conflicts, and the hierarchical taxonomy handling. Moreover, what is the resource-efficient way to utilize emerging large pre-trained vision models for million-scale cross-dataset object detection remains an open challenge. This paper tries to address these challenges by introducing our practices in label handling, hierarchy-aware loss design and resource-efficient model training with a pre-trained large model. Our method is ranked *second* in the object detection track of Robust Vision Challenge 2022 (RVC 2022). We hope our detailed study would serve as an alternative practice paradigm for similar problems in the community. The code is available at <https://github.com/linfeng93/Large-UniDet>.

Keywords: universal object detection, large vision model, resource-efficient, hierarchical taxonomy

1 Introduction

A broad, universal, and general-purpose computer vision system becomes a trend in the development of computer vision (Gong, Dai, Chen, Li, & Van Gool, 2021; Hasan, Liao, Li, Akram, & Shao, 2021; Y. He et al., 2022; Wang, Cai, Gao, & Vasconcelos, 2019; X. Zhou, Koltun, & Krähenbühl, 2022). This universal vision model is a multi-skilled agent capable of solving various vision tasks

simultaneously without much human intervention. With that, researchers no longer have to train individual models each for a specific vision task or finetune an existing model for a particular data domain. They can simply complete all the tasks with one effort. This model universality is likely a promising direction for human-like AI and has great significance in real-world computer vision applications (Yuan et al., 2021).

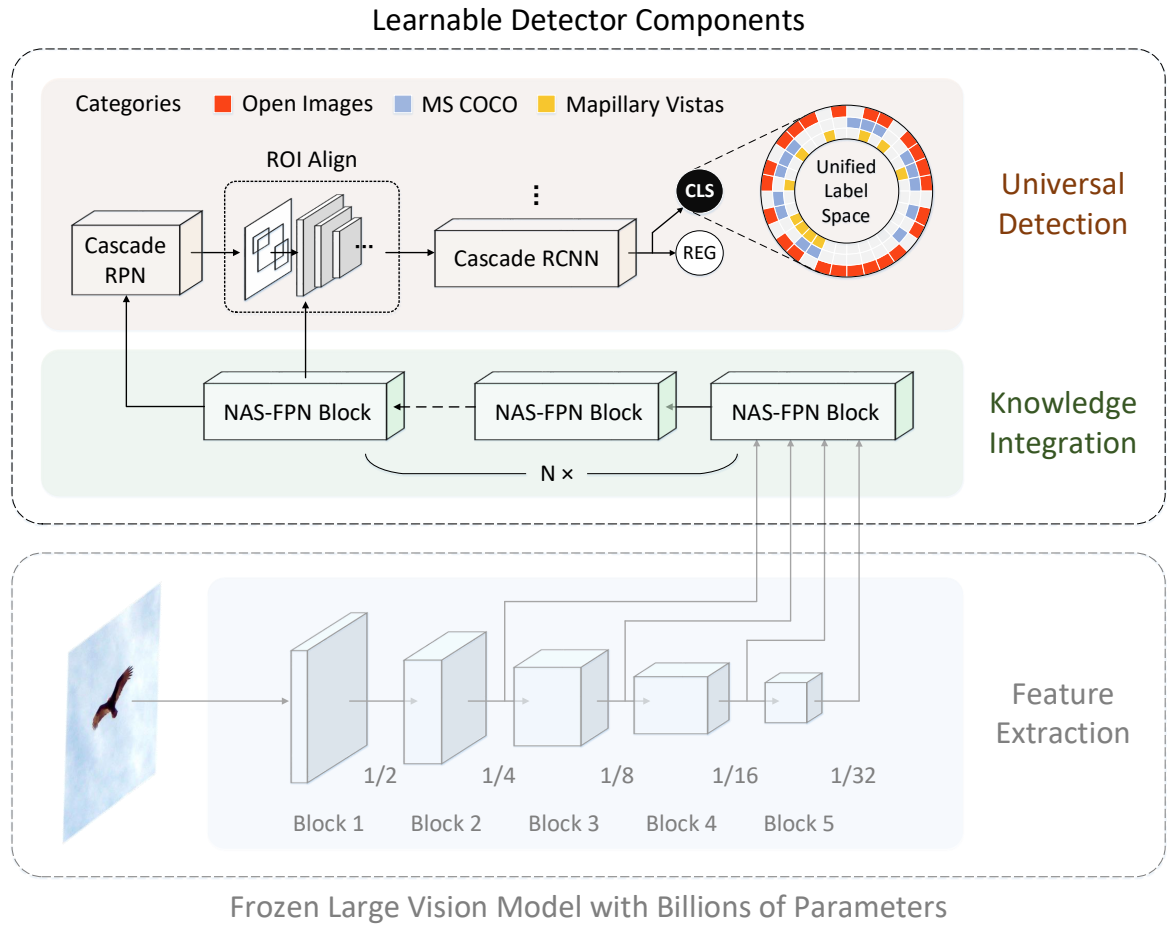


Fig. 1 Overview. The design of Large-UniDet is based on a two-stage RCNN-style object detection network. The frozen backbone is a RegNet architecture initialized with the weights of SEER models. The NAS-FPN blocks can be stacked N times for a better accuracy-cost trade-off. The classification branch of Cascade R-CNN outputs 541 class scores including the *background* as the cardinality of the unified label space is 540.

In this study, we take a concrete step toward the universal vision technologies, mainly focusing on the million-scale universal object detection problem across different domains. Without prior knowledge of the dataset of interest, the universal object detector conducts the inference procedure once to generate unified detection results across all datasets, which potentially have very different domain characteristics.

Toward the million-scale multi-domain universal object detection problem, there are two primary difficulties, including (a) the cost of curating such a large-scale training dataset and (b) the modeling approach to obtain robust visual representations. Specifically, to achieve satisfactory

results across domains, a large-scale dataset covering all kinds of data domains is indispensable in the training stage. Nevertheless, we do not have such a dataset to satisfy the data needs. Besides, for object detection (Zhao et al., 2020; X. Zhou et al., 2022) or similar fine-grained computer vision tasks (Bevandić & Šegvić, 2022; Lambert, Liu, Sener, Hays, & Koltun, 2020; Ranftl, Lasinger, Hafner, Schindler, & Koltun, 2020), it is prohibitively expensive to build a unified large-scale dataset consisting of diverse scenes with a tremendous amount of dense annotations. In terms of robust representations, it is not so trivial to satisfy the demand of the robustness to the million-scale various source data in a common object detector

since the objects of interest appearing in a wide variety of images could vary greatly.

Fortunately, with the increasing availability of various detection datasets worldwide, researchers have an opportunity to implement universal object detectors by reusing off-the-shelf datasets jointly. We leverage the existing datasets by unifying the independent label spaces of each used dataset. With the proposed unified label space, we are able to handle multi-domain object detection with different label vocabularies. Multiple diverse datasets could lead to annotation inconsistency problems like label duplication, label conflicts, and incomplete hierarchical taxonomy. We design an elaborate loss formulation in the unified label space to address these problems.

To achieve robustness to the million-scale data, we turn to the emerging large vision pre-training. Some recent works have validated the great significance of large models for learning better visual representations (Bello et al., 2021; Radosavovic, Kosaraju, Girshick, He, & Dollár, 2020). Trained on the same data, the larger models could capture higher-quality visual representations, superior to that of the smaller counterparts (Kolesnikov, Zhai, & Beyer, 2019). These higher-quality visual representations could also lead to better in-domain and out-of-domain generalization (Goyal et al., 2022). For this reason, we hypothesize the universal object detection aiming at million-scale diverse datasets would benefit significantly from the large models, especially the well-trained ones. We did observe in the experiments utilizing larger vision models indeed improves universal object detection in performance by an impressive gain, even with a vast training set.

As we acquire the feature robustness by taking advantage of large pre-trained vision models, computational resources become a critical demand because of both computational and memory-wise costs. Without many computational resources yet, we introduce a resource-efficient training formulation for large vision models inspired by a recent work (Vasconcelos, Birodkar, & Dumoulin, 2022), which saves considerable computational resources, especially GPU memory, during the training procedures.

This paper presents our practices for million-scale multi-domain universal object detection with the help of the emerging large pre-trained vision models. Due to the efficient formulation design,

elaborate label handling, and knowledge transfer from large-scale pre-training, our method, Large-UniDet, achieves impressive performance. It wins the second prize in the object detection track of Robust Vision Challenge 2022¹. Our contributions are summarized as follows.

- We provide practices in using large vision models in million-scale universal object detection.
- We present a resource-efficient training formulation for universal object detection with limited computational resources.
- With the unified label space, we design a loss strategy to overcome cross-dataset label duplication and semantic hierarchy problems.
- The proposed method achieved the 2nd prize in the object detection track of RVC 2022.

2 Related Works

2.1 Universal Object Detector

Universal object detection has been widely studied in very recent years. Wang et al. (Wang et al., 2019) propose a universal detector with a domain attention module that leverages shared knowledge across different data domains. Essentially, their design is multiple dataset-specific detectors that share most network parameters since the output predictions keep the categories of each dataset separate from each other. Considering the semantic correlations over various datasets, Universal-RCNN (Xu, Fang, Liang, Kang, & Li, 2020) tries to incorporate graph transfer learning for modeling the intra-domain and inter-domain semantics of categories from three datasets (Krishna et al., 2017; T.-Y. Lin et al., 2014; B. Zhou et al., 2017). From another perspective, without different specifications of network structures for each dataset, Zhao et al. (Zhao et al., 2020) build a unified label space by manually merging multiple label spaces of different datasets. Their proposed framework is dedicated to managing with partial annotations by the pseudo-labeling approach. To avoid manual efforts for the merged unified taxonomy, UniDet (X. Zhou et al., 2022) presents an automatic method to unify the label spaces of multiple datasets on the basis of visual concepts. The visual concepts are generated by the partitioned object

¹www.robustvision.net/leaderboard.php?benchmark=object, IFFF_RVC entry on Leaderboard

detector with three separate detection branches. Using a language model (Devlin, Chang, Lee, & Toutanova, 2018), Cai et al. (L. Cai et al., 2022) extract category embedding for each dataset to construct a unified label space. Recently, Meng et al. (Meng et al., 2022) firstly leverage pre-trained language embedding to produce adapted queries for each category embedding on different datasets. They model object classification as a region-word alignment problem without a merged unified label space.

Similar to the methods mentioned above based on the unified label spaces, we propose a universal object detector with an improved hierarchical taxonomy that is simply modified from the RVC official manually-crafted taxonomy. Besides, the proposed hierarchy-aware cross-dataset loss suppression overcomes the label duplication and semantic hierarchy problems caused by multiple merged datasets.

2.2 Pre-training for Vision Tasks

Pre-training is a common practice in many computer vision tasks (Azizi et al., 2021; L. Cai et al., 2022; Caron et al., 2020; Joulin, Maaten, Jabri, & Vasilache, 2016; Kornblith, Shlens, & Le, 2019; Sun, Shrivastava, Singh, & Gupta, 2017), yielding remarkable improvement in performance with the backbones pre-trained on large-scale labeled or unlabeled datasets, such as ImageNet (Deng et al., 2009), JFT-300M (Sun et al., 2017), OpenImages (Kuznetsova et al., 2020), and unlabeled web-collected data (Goyal et al., 2022). A well-trained backbone could generate more robust visual representations, which can benefit downstream vision tasks in some specific data domains (Goyal et al., 2022). For object detection, the initialized backbone as a feature extractor significantly connects with the performance (Y. Liu et al., 2020). Generally, the robust pre-trained backbones come from (a) stronger architectures with high capacity, (b) broader training datasets, and (c) more advanced pre-training manners.

Stronger architecture. To reveal the influence of backbone architectures, Huang et al. (Huang et al., 2017) investigate the correlation between the backbone capacities and object detection performance. Liu et al. (Y. Liu et al., 2020) assemble multiple identical backbones to construct a stronger backbone. In view of the powerful vision

transformers, Liu et al. (Z. Liu et al., 2022) build an extremely large object detector by utilizing an expanded swin transformer as the feature extractor. A lot of literature explores the model design targeted to higher performance for object detection. No more related works are listed here for lack of space.

Training data. From the perspective of training data, Sun et al. (Sun et al., 2017) improve robust representation learning with a large-scale dataset JFT-300M. Bu et al. (Bu, Peng, Yan, Tan, & Zhang, 2021) use the union of various detection datasets (Dollar, Wojek, Schiele, & Perona, 2011; Kuznetsova et al., 2020; T.-Y. Lin et al., 2014; S. Shao et al., 2019; Zhang, Benenson, & Schiele, 2017) to obtain well-adapted pre-trained weights of object detectors for downstream transfer learning. Cai et al. (L. Cai et al., 2022) leverage the existing detection datasets (Gupta, Dollar, & Girshick, 2019; Kuznetsova et al., 2020; S. Shao et al., 2019) to build a large pre-training dataset by curating the data with carefully designed principles. For space limitations, more similar works are not covered here.

Pre-training approach. Many recent advances in model pre-training (Caron et al., 2020; K. He et al., 2022; K. He, Fan, Wu, Xie, & Girshick, 2020; F. Lin, Xu, Li, Xiong, & Qi, 2021; Xu et al., 2022) show self-supervised methods are surpassing supervised counterparts in downstream tasks like object detection, semantic segmentation, and image classification. Without relying on manual annotations, self-supervised pre-training methods have the potential to capture more discriminative visual representations with unlimited diverse web-scale image data (Goyal et al., 2022). In addition, vision foundation models (Jia et al., 2021; Radford et al., 2021; J. Shao et al., 2021; Yuan et al., 2021) trained on web-scale image-text data demonstrate the significant influence of representation learning in the in-domain and out-of-domain downstream tasks.

In light of the success of model pre-training, we use large self-supervised vision models, namely the SEER models (Goyal et al., 2022), as the backbones of our universal object detector. As mentioned above, robust backbones benefit from high-capacity architectures, broad training data, and advanced pre-training approaches. As requested, the largest SEER model contains 10 billion network parameters. The SEER models are trained

on 1 billion less biased uncuration images collected from web images by a self-supervised clustering-based method (Caron et al., 2020), producing more robust visual representations on in- and out-of-domain benchmarks (Goyal et al., 2022). We believe the SEER backbones can generate more discriminative features and also lead to better out-of-distribution generalization for the challenge of universal object detection on a variety of datasets with different characteristics.

3 Method

3.1 Resource-efficient Detection with a Large Vision Model

This section presents a strong object detector built on the large pre-trained backbone networks. Large vision models have been proven to be beneficial for many downstream computer vision tasks. However, the astonishing hardware requirements (Dai, Liu, Le, & Tan, 2021; Radford et al., 2021; J. Shao et al., 2021) for training a large model prevent its broad application. In order to utilize a large vision model with limited hardware access, we propose a computation & memory efficient training formulation which freezes the billions of backbone parameters and then adapts the extracted visual representations to the subsequent detector components. By the proposed technique, we are able to train our largest model on 16 NVIDIA 3090 GPUs. We believe that our practices in leveraging a large vision model would benefit the community interested in investigating large-scale object detection with limited computational resources. This resource-efficient approach is inspired by the recent progress in knowledge transfer (Vasconcelos et al., 2022) but is specially focused on large pre-trained vision models.

Fig. 1 illustrates the overall framework. Each detector component is described in detail in the remaining content of this section.

3.1.1 Frozen Backbone with Billions of Parameters

Considering the SEER model (Goyal et al., 2022) has been proven more fair and less biased on different domains, we employ the released SEER model as the backbone in our object detection network for the robust visual representations across three

quite different datasets, *i.e.* MS COCO (COCO), OpenImages Dataset (OID), and Mapillary Vistas Dataset (MVD). As well known, the conventional practice to optimize object detectors is to fine-tune both the initialized backbone and subsequent detector components on detection datasets. However, finetuning the backbone on relatively smaller detection datasets will cause the backbone parameters to drift away from their pre-trained initialization, which may degrade the detection performance (Vasconcelos et al., 2022). Furthermore, finetuning the parameters of a heavy backbone will cause much higher computational complexity. Consequently, to obtain superior detection performance while managing the computational complexity, we freeze the backbone parameters during the training procedure. This efficient formulation is not only simple and resource-saving but also has a clear positive impact on the long-tailed object categories owing to knowledge preservation (Vasconcelos et al., 2022), which is helpful in the RVC multi-domain scenario.

The released SEER models are trained on billions of uncuration internet images. It is observed their in-domain and out-of-domain generalization increases with the model size consistently (Goyal et al., 2022). Considering the trade-off between cost and performance, we utilize a lighter version (SEER-RegNet32gf) and the second largest version (SEER-RegNet256gf) in the extensive experiments and our RVC final submission.

3.1.2 Cascade Detection Heads

Based on the frozen SEER backbone, we adopted a two-stage RCNN-style detection framework. In our preliminary experiments, Faster R-CNN (Ren, He, Girshick, & Sun, 2015) fails to achieve satisfactory performance. A possible reason is there are minimal learnable parameters in the object detector, and it is too challenging for such an object detector to deal with the million-scale detection across diverse datasets. Inspired by some recent works (Vasconcelos et al., 2022), we employ high-capacity Cascade R-CNN (Z. Cai & Vasconcelos, 2018) as our detection heads, which dramatically boosts performance, detailed in Section 4.5.1.

3.1.3 Stacked Dense Neck

Feature pyramid network (FPN) is a basic component in an object detection framework, serving as

an adaptation module to incorporate and enhance hierarchical features, just like the neck that connects the backbone and the subsequent detection heads. As the first attempt, the FPN (T.-Y. Lin et al., 2017) transfers multi-level semantic knowledge from the backbones by a top-down pathway and lateral connections. This common-used design only produces a simple, straightforward path for knowledge incorporation. At the same time, the follow-ups (Ghiasi, Lin, & Le, 2019; S. Liu, Qi, Qin, Shi, & Jia, 2018; Pang et al., 2019; Tan, Pang, & Le, 2020) introduce cross-scale connections to enhance visual representations with semantically vital information and low-level cues.

We employ a stacked, densely connected FPN, namely NAS-FPN (Ghiasi et al., 2019), as the neck of our object detector for the following four reasons.

- As universal object detection is to detect hundreds of object categories from various datasets, the impressive ability of NAS-FPN to generate robust representations meets the challenges of million-scale multi-domain detection.
- As we freeze the backbone, the remaining detector components require higher model capacity (described in Section 3.1.2), while stacked NAS-FPN offers excellent flexibility in constructing rich neck architecture.
- The released SEER models are trained on billions of uncurated web-scale images. Inevitably, there is some domain gap between the upstream pre-training dataset and downstream detection datasets. As we do not finetune the SEER models on the downstream data, we believe the early NAS-FPN blocks can act as domain adaptors to align the domain gap.
- Last but not least, we observe that multi-level side-outputs of SEER models have very different characteristics. Some shallow side-outputs are dense, while the deeper ones are generally sparse and weak. The rich connections of NAS-FPN offer more possible ways for better feature integration.

3.1.4 Adaptive RPN

In the multi-domain object detection scenario, the objects sharing the same taxonomy have different characteristics across domains. For instance, the object *person* appearing in autonomous driving datasets, such as MVD, is usually tiny against

the high-resolution street scenes, while the *person* appearing in the COCO images is usually much bigger. Very obviously, the object sizes of different domains can vary greatly. In order to obtain precise predictions for the diverse objects of varying sizes, we employ an adaptive RPN, namely Cascade RPN (Vu, Jang, Pham, & Yoo, 2019), to provide more high-quality region proposals without heuristically investigating appropriate scales and aspect ratios for pre-defined anchors. Moreover, over-sufficient pre-defined anchors even slow the network training. Apart from sweetening the proposals, Cascade RPN can further increase the model capacity, making the best of both worlds.

3.2 Cross-dataset Model Training

3.2.1 Label Space Unification Across Multiple Datasets

In this section, we introduce the unified label space for three datasets. Also, we describe the existing problems caused by label duplication and semantic hierarchy across datasets. For a good starting point, RVC organizers provide a manually-crafted taxonomy². According to the RVC official taxonomy, each category from either COCO or MVD has been remapped to one category in the RVC official unified label space, and so does each leaf-node category from OID. However, the non-leaf categories from OID are not included. In order to obtain a complete label space, we modify this flat official taxonomy by simply appending all OID’s non-leaf categories apart from the root entry. As a result, the cardinality of our unified label space is 540.

According to the original semantic hierarchy of OID, the appended superclasses, *i.e.*, non-leaf categories, are more general than other classes. This granularity inconsistency correspondingly results in cross-dataset label duplication and semantic hierarchy problems. For example, the superclass *person* (/m/01g317) from OID and the class *person* from COCO remain two independent categories, although both are semantically identical. For another example, the class *cow* from COCO belongs to the superclass *animal* (/m/0jbk) from OID in semantics, but OID’s semantic hierarchy does not reflect this parent-child structure. These

²https://github.com/ozendelait/rvc_devkit/blob/master/objdet/obj_det_mapping.csv

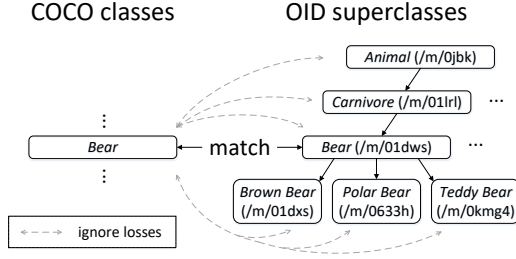


Fig. 2 An example shows the loss suppression for semantically label duplication between COCO and OID.

unexpected semantic overlaps in taxonomy may degrade universal object detection performance. To handle label duplication and semantic hierarchy, we apply a unified hierarchical taxonomy and utilize hierarchy-aware loss suppression dedicated to multiple datasets, detailed in Section 3.2.2 and 3.2.3, respectively.

3.2.2 Multi-label with Hierarchical Taxonomy Completion

We describe hierarchical taxonomy completion to deal with the semantic hierarchy of OID in addition to the merged categories by the RVC official taxonomy and leave the rest tricky cross-dataset semantic hierarchy to Section 3.2.3.

We convert the one-hot category labels to the multi-class labels by setting all their parent categories as positives for the OID images, similar to UniDet (X. Zhou et al., 2022). But unlike UniDet,

Two categories match in semantics	
COCO classes	OID superclasses
<i>sports ball</i>	<i>ball</i> (/m/018xm)
<i>bear</i>	<i>bear</i> (/m/01dws)
<i>bed</i>	<i>bed</i> (/m/03ssj5)
<i>bird</i>	<i>bird</i> (/m/015p6)
<i>boat</i>	<i>boat</i> (/m/019jd)
<i>car</i>	<i>car</i> (/m/0k4j)
<i>clock</i>	<i>clock</i> (/m/01x3z)
<i>person</i>	<i>person</i> (/m/01g317)
MVD classes	OID superclasses
<i>object-vehicle-car</i>	<i>car</i> (/m/0k4j)
<i>human-person</i>	<i>person</i> (/m/01g317)

Table 1 The duplicated category names between OID superclasses and COCO / MVD classes in semantics.

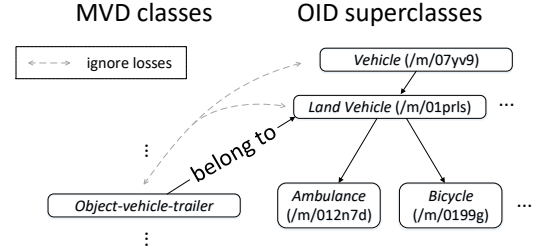


Fig. 3 An example shows the loss suppression for semantic hierarchy between MVD and OID.

which only considers the OID images, we incorporate semantic hierarchies of COCO and MVD with the aid of the semantic hierarchy of OID. To be specific, for each annotated box whose ground truth category has been already merged with an OID leaf-node category according to the RVC official taxonomy, we treat it as its OID equivalent. For example, observing the COCO *banana* and the OID *banana* (/m/09qck) are merged into a single mutual category, for a bounding box annotated as *banana* from COCO, we assign the category *fruit* a positive label because the class *banana* belongs to the superclass *fruit* per the semantic hierarchy of OID. We use a multi-label classifier in detection

The left as a descendant of the right in semantics	
COCO classes	OID superclasses
<i>cow</i>	<i>animal</i> (/m/0j bk)
MVD classes	OID superclasses
<i>animal-ground</i>	<i>animal</i> (/m/0j bk)
<i>-animal</i>	
<i>object-vehicle</i>	<i>land vehicle</i> (/m/01prls)
<i>-caravan</i>	
<i>object-vehicle-other</i>	<i>land vehicle</i> (/m/01prls)
<i>-vehicle</i>	
<i>object-vehicle-trailer</i>	<i>land vehicle</i> (/m/01prls)
<i>object-vehicle</i>	<i>land vehicle</i> (/m/01prls)
<i>-wheeled-slow</i>	
<i>object-support-traffic</i>	<i>traffic sign</i> (/m/01mqdt)
<i>-sign-frame</i>	
<i>object-traffic-sign</i>	<i>traffic sign</i> (/m/01mqdt)
<i>-back</i>	
<i>object-traffic-sign</i>	<i>traffic sign</i> (/m/01mqdt)
<i>-front</i>	

Table 2 The parent-child category names between OID superclasses and COCO / MVD classes in semantics.

$$L_{rpn} = \frac{1}{N} \sum_{i=0}^N \sum_{s=0}^{S_{rpn}} (\alpha \cdot (1 - IoU(p_s^i, y_{rloc}^i)) + BCE(q_s^i, y_{rcls}^i)) \quad (1)$$

$$L_{head} = \frac{1}{N} \sum_{i=0}^N \sum_{s=0}^{S_{head}} (\beta \cdot SmoothL_1(r_s^i, y_{loc}^i) + \frac{\gamma}{C} \cdot \sum_{c=0}^C L_{cls}^c) \quad (2)$$

$$L_{cls}^c = (1 - \mathbb{1}_{\mathcal{D}(y_{cls}^i)}(c)) \cdot BCE(x_s^{ic}, \mathbb{1}_{\mathcal{P}(y_{cls}^i)}(c)) \quad (3)$$

heads to obtain the class confidences by *sigmoid* activation functions for each bounding box.

It is worth noticing that this hierarchical taxonomy completion is still incomplete. There are a number of COCO / MVD annotated objects whose ground truth category does not match any OID leaf-node category but semantically belongs to a certain superclass from OID. We do not activate the corresponding parent categories, instead handle these semantic hierarchies by an elaborate adaption in the loss function detailed in the next section.

3.2.3 Hierarchy-aware Cross-dataset Loss Suppression

Given label duplication described in Section 3.2.1 and unsolved semantic hierarchies described in Section 3.2.2, we elaborate a loss adaption strategy named hierarchy-aware cross-dataset loss suppression (HCLS) to address both simultaneously. Based on the semantic hierarchy of OID, HCLS ignores the losses over the categories involved with label duplication and semantic hierarchy between OID and COCO / MVD in the box classification branches. More specifically,

- For each category from OID, HCLS ignores the losses over all its child categories, as a common practice for hierarchical taxonomy (Kuznetsova et al., 2020).
- For each category from COCO / MVD, which is not merged with any OID leaf-node category in the RVC official taxonomy, HCLS searches all the superclasses from OID and performs one of the following adaptations to the loss:

(a) [Label duplication] Suppose this category matches one of the superclasses from OID in semantics. In this case, HCLS ignores the loss

between its OID equivalent and itself, in addition to the losses between its OID equivalent's parents/children and itself.

(b) [Cross-dataset semantic hierarchy] Suppose this category belongs to one of the superclasses from OID in semantics. HCLS ignores the losses between all its parent categories and itself.

(c) [Neither] Suppose this category is independent of any superclass of OID. HCLS does nothing about loss adaptation. In other words, we equally calculate losses over all the categories in the unified label space in loss functions.

In Fig. 2 and Fig. 3, two examples illustrate the loss adaptation process (a) and (b), respectively. Note that we do **not** perform any laborious category merging, but handle label duplication on loss levels. According to the RVC official taxonomy, the number of categories independent of OID is less than fifty, so we manually search for cross-dataset label duplication and semantic hierarchy. Please refer to Table 1 for the processed semantically duplicate categories and Table 2 for the processed semantic hierarchies across datasets.

3.2.4 Overall Formulation

The overall loss function can be formulated as the weighted sum of the RPN loss and the detector head loss, described as follows,

$$L = \lambda \cdot L_{rpn} + L_{head} \quad (4)$$

where λ is the weight factor set to 0.7, while L_{rpn} represents the RPN loss (1) and L_{head} represents the detector head loss (2). In the detector head loss L_{head} , the classification loss L_{cls} is given in (3).

In formulas (1), (2), and (3), the symbols p , q , r , and x denote the respective outputs for RPN regression branch, RPN classification branch, the detector head regression branch, and the detector head classification branch, while the y denotes the corresponding ground truth. N is the number of samples in each mini-batch. C is the number of categories including *background* in the unified label space. S_{rpn} represents the number of stages of Cascade RPN while S_{head} represents the number of stages of Cascade R-CNN. We set S_{rpn} to 2 and S_{head} to 3 for a performance-cost trade-off reason. IoU represents the IoU loss (Yu, Jiang, Wang, Cao, & Huang, 2016), BCE represents the binary cross entropy loss, and $SmoothL_1$ represents the smooth L1 loss. $\mathbb{1}_{\mathbb{A}}(x)$ represents the indicator function in which the result turns out 1 when $x \in \mathbb{A}$. Specifically, $\mathbb{D}(y)$ denotes the union of the categories involved in HCLS for class y , as described in Section 3.2.3. $\mathbb{P}(y)$ denotes the union of the parent categories of class y as described in Section 3.2.2. The loss weights α , β , and γ are set to 10.0, 1.0, and 1.5, respectively.

4 Experiments

4.1 Datasets

Three used datasets are summarized in Table 3. COCO (T.-Y. Lin et al., 2014) is collected from images of everyday objects and humans, including 80 common object categories. MVD (Neuhold, Ollmann, Rota Bulo, & Kontschieder, 2017) is a diverse high-resolution imagery dataset. Its version of 1.2, which includes 37 street-scene object categories, is used in our experiments and RVC 2022. Different from the flat taxonomies in COCO and MVD, OID (Kuznetsova et al., 2020) is annotated with a semantic hierarchy. The images from OID are very diverse and often contain complex scenes with several objects. In addition, the annotated classes have a long-tailed distribution. We use its training set with 500 object categories as a standard practice in Open Images Challenge 2019.

4.2 Implementation Details

The proposed method is implemented with mmdetection (Chen et al., 2019) codebase. As mentioned in Section 3.1, we design a resource-efficient training formulation with the frozen SEER-RegNet32gf

Dataset	Domain	# Cats	# Imgs
COCO	Internet images	80	118k
MVD	Street scenes	37	1.8k
OID	Internet images	500	1.8M

Table 3 The training datasets used in the experiments, which are provided by organizers of RVC 2022.

and SEER-RegNet256gf as the backbones. As for the subsequent learnable detector components, we convert BatchNorm (BN) to synchronized BatchNorm (SyncBN) for synchronizing statistics across total GPU workers. Unless otherwise specified, the hyper-parameters we adopt in NAS-FPN, Cascade RPN, and Cascade R-CNN remain default as their official implementations.

We apply standard data augmentation, including random flip and random scaling of the short edge in a range [480, 960]. We utilize SGD optimizer to train our models with a base learning rate of 0.01, weight decay of 0.0001, and a batch size of 16. To alleviate the imbalance problems caused by the long-tailed class distribution and the vastly different sizes of 3 datasets, the class-aware sampling and the dataset-wise re-sampling techniques are applied when training universal object detectors. The sampling ratio of the dataset-wise re-sampling is set to 1: 4: 8 for OID, COCO, and MVD. The models are trained on 8 NVIDIA 3090 / A100 GPUs. Mixed-precision technique (Micke-vicius et al., 2018) is always applied to accelerate model training. Unless specified, the short edge of the images is resized to 800 while the long edge of that is restricted to 1333 without changing the aspect ratio during the inference procedure.

4.3 RVC Submission

For our RVC final submission, the detector is built on SEER-RegNet256gf, while the model implementation is a little different from that in this paper. In order to meet the RVC deadline, we made a few simplifications for the model used in the challenge:

- We employed side-outputs $\{C_3, C_4, C_5\}$ instead of the default setting $\{C_2, C_3, C_4, C_5\}$ in NAS-FPN and then performed the $2\times$ downsampling on C_5 twice to build a 5-level feature pyramid. This simplification has adversely affected the

Methods	COCO <i>test</i>		COCO <i>val</i>		MVD <i>test</i>		MVD <i>val</i>		OID <i>test</i>	OID <i>val</i>
	mAP	AP50	mAP	AP50	mAP	AP50	mAP	AP50	AP50	AP50
MD_RVC (1)	59.0	76.0	-	-	32.8	49.3	-	-	62.1	-
IFFF_RVC (2)	50.0	69.0	50.0	69.1	25.3	39.0	24.2	38.6	59.9	69.1
USTC_RVC (3)	50.0	68.0	-	-	25.1	37.9	-	-	47.8	-
CBS_RVC (4)	48.0	66.0	-	-	13.5	21.5	-	-	47.7	-
TSDREF_RVC (5)	19.0	31.0	-	-	6.6	11.6	-	-	40.2	-
Large-UniDet [S]	-	-	48.8	66.2	-	-	25.9	39.4	-	68.5
Large-UniDet [L]	-	-	51.9	70.0	-	-	27.7	42.2	-	69.8
Large-UniDet [S] [†]	-	-	52.0	70.4	-	-	32.0	47.8	-	69.2
Large-UniDet [L] [†]	-	-	53.5	71.8	-	-	33.2	49.4	-	70.5

Table 4 Comparisons on five RVC submissions on three datasets, the numbers in brackets denote the achieved places in the challenge. The last four rows report our new results in this paper, we only provide the accuracy on validation sets as the RVC test server is off after RVC deadline. Large-UniDet [S] indicates our method based on SEER-RegNet32gf while Large-UniDet [L] indicates the one based on SEER-RegNet256gf. The training of both [S] and [L] starts with the base learning rate of 0.01, which is warm-uped in the preceding 4k iterations and is decreased by a factor of 10 at 850k and 1.0M iterations, and stop at 1.15M iterations. Additionally, the following finetune detailed in Section 4.5.4 is conducted, whose results are distinguished by superscript [†].

detection of those tiny objects but did save the training time considerably.

- The basic anchor scale was reduced to 5.04 ($4 \times 2^{1/3}$) in Cascade RPN to align with the changes in NAS-FPN, alleviating the missed detection problem for tiny objects.
- The model was trained for 720k iterations, with the learning rate dropped at 600k iterations by a factor of 0.1.

During the dataset-agnostic inference procedure, the Soft-NMS (Bodla, Singh, Chellappa, & Davis, 2017) was performed with an IoU threshold of 0.6 and a score threshold of 0.001, then,

- for COCO, the max number of predictions per image was restricted to 100, the short edge of the input image was resized to 800.
- for MVD, the max number of predictions per image was restricted to 300, the short edge of the input image was resized to 2048.
- for OID, the max number of predictions per image was restricted to 300, the short edge of the input image was resized to 800.

We did **not** apply any elaborate inference strategy like multi-scale test augmentation. The results of our submission (IFFF_RVC) on three datasets are reported in Table 4. For comparison with the results of this paper, we evaluate the model for our RVC submission on the validation sets where the

max number of predictions per image is always set to 300 with performing the common NMS instead. Besides, other testing configurations are kept the same as that used on test sets.

4.4 Main Results

Comparisons on the RVC final submissions, as well as our new results, are summarized in Table 4. The ranked #1 MD_RVC employs a large transformer-based object detector (Carion et al., 2020) with an acceleration training strategy that increases the input size progressively. From another perspective, our method, named Large-UniDet, is devoted to building a computation & memory-saving training formulation and generating robust multi-domain object detection predictions by taking advantage of large pre-trained vision models.

Compared to our RVC submission IFFF_RVC, Large-UniDet isn't simplified as the description in Section 4.3 and is further improved with a training practice where the model is adapted for the high resolution of input data (detailed in Section 4.5.4). As we can see in Table 4, based on a lighter backbone (SEER-RegNet32gf), Large-UniDet achieves 48.8, 66.2, 25.9, 39.4, and 68.5 points in terms of mAP on COCO *val* set, AP50 on COCO *val* set, mAP on MVD *val* set, AP50 on MVD *val* set, and AP50 on OID *val* set, respectively. The larger

Model	mAP	Time (h)
Faster R-CNN	29.0	12
Cascade R-CNN	39.9	13
+ PAFPN	40.8 (+0.9)	16 (+3)
+ Cascade RPN	42.0 (+2.1)	19 (+6)
+ BiFPN (×1)	40.5 (+0.6)	16 (+3)
+ BiFPN (×3)	41.5 (+1.6)	18 (+5)
+ BiFPN (×5)	41.3 (+1.4)	20 (+7)
+ BiFPN (×7)	41.1 (+1.2)	22 (+9)
+ Cascade RPN	42.1 (+2.2)	25 (+12)
+ NAS-FPN (×1)	41.6 (+1.7)	16 (+3)
+ NAS-FPN (×3)	44.2 (+4.3)	18 (+5)
+ NAS-FPN (×5)	45.3 (+5.4)	20 (+7)
+ NAS-FPN (×7)	45.7 (+5.8)	22 (+9)
+ Cascade RPN	47.6 (+7.7)	24 (+11)

Table 5 Ablation analysis of detector components on COCO *val* set. The models are trained for 12 epochs on 8 NVIDIA 3090 GPUs, with a base learning rate 0.01 which is divided by 10 after 8 and 11 epochs.

backbone (SEER-RegNet256gf) improves universal object detection in performance consistently (+3.1 mAP / 3.8 AP50 on COCO, +1.8 mAP / 2.8 AP50 on MVD, +1.3 AP50 on OID), which does demonstrate the effectiveness of visual representations generated by larger vision models. Without the simplifications in our RVC submission, Large-UniDet [S] and [L] are trained for 1.15M iterations, longer than the IFFF_RVC, with the base learning rate which is linearly warm-upped in the preceding 4k iterations and decreased by a factor of 10 at 850k and 1.0M iterations. When testing, we generate no more than 300 predictions per image with the common NMS for a fair comparison with the IFFF_RVC on validation sets.

After the universal object detection training, we conduct the dataset-specific individual fine-tuning with the high-resolution training images, detailed in Section 4.5.4. This practice can further improve the performance of three datasets, especially on MVD, which has fairly different characteristics compared with the other two datasets. The detailed AP numbers are shown in Table 4, denoted as Large-UniDet with superscript [†].

Model	mAP	Time (h)
Faster R-CNN	12.8	1.8
Cascade R-CNN	15.2	2.0
+ PAFPN	16.7 (+1.5)	2.5 (+0.5)
+ Cascade RPN	17.3 (+2.1)	3.5 (+1.5)
+ BiFPN (×1)	17.0 (+1.8)	2.5 (+0.5)
+ BiFPN (×3)	17.1 (+1.9)	2.8 (+0.8)
+ BiFPN (×5)	16.8 (+1.6)	3.1 (+1.1)
+ BiFPN (×7)	16.5 (+1.3)	3.4 (+1.4)
+ Cascade RPN	16.7 (+1.5)	4.3 (+2.3)
+ NAS-FPN (×1)	17.3 (+2.1)	2.8 (+0.8)
+ NAS-FPN (×3)	18.3 (+3.1)	3.0 (+1.0)
+ NAS-FPN (×5)	18.6 (+3.4)	3.2 (+1.2)
+ NAS-FPN (×7)	19.4 (+4.2)	3.5 (+1.5)
+ Cascade RPN	20.2 (+5.0)	4.2 (+2.2)

Table 6 Ablation analysis of detector components on MVD *val* set. For fast convergence, we initialize the models with the counterparts in Table 5, and train them for 12 epochs on 8 NVIDIA 3090 GPUs, with a base learning rate 0.01 which is divided by 10 after 8 and 11 epochs.

4.5 Ablation Study

4.5.1 Detector Components Analysis

We conduct the ablation analysis based on SEER-RegNet32gf. Table 5 and Table 6 report accuracy-cost comparisons about different detector configurations on COCO and MVD, respectively. With a frozen backbone, Cascade R-CNN outperforms the baseline Faster R-CNN by a significant margin, improving the mAP to 39.9 on COCO while 15.2 on MVD with a little increased training cost (+1 hour for COCO and +0.2 hour for MVD).

When integrating the high-capacity necks into Cascade R-CNN, we achieve higher accuracy but simultaneously suffer the increasing computation burden. Three frequently used FPNs are compared in Tables 5 and 6. As we can see, PAFPN (S. Liu et al., 2018) yields 0.9 and 1.5 points improvement, and BiFPN (Tan et al., 2020) yields at most 1.6 and 1.9 points improvement on COCO and MVD, respectively. As a better choice, NAS-FPN yields 5.8 and 4.2 points improvement. Tables 5 and 6 show that the computational cost increases with the number of stacked neck blocks. At the same time, the performance growth is gradually decelerated, and even the performance degrades for the

Loss Strategy	COCO	MVD	OID
Baseline	36.2	<u>14.4</u>	61.7
Naive loss suppression	<u>36.4</u>	14.5	62.7
Unified hierarchy	36.3	14.0	<u>64.8</u>
OID hierarchy	<u>36.4</u>	14.0	<u>64.8</u>
+ HCLS	37.1	14.3	65.2

Table 7 Comparison on loss strategies. The used object detector is Cascade R-CNN based on SEER-RegNet32gf. The five models are trained for 420k iterations, with a base learning rate 0.01 which is decayed by a factor of 0.1 at 280k iterations. Note that the metric of COCO and MVD is mAP and the metric of OID is AP50. The best and the second best results are highlighted in **bold font** and under line, respectively.

stacked BiFPN. Consequently, we equip our detector with seven stacked NAS-FPN blocks, enjoying a good trade-off between accuracy and cost.

Besides, Cascade RPN brings a consistent gain (+1.0 mAP at least on COCO and +0.2 mAP at least on MVD) across whatever necks, especially for NAS-FPN, without increasing too much extra computational cost.

4.5.2 Hierarchical Loss Strategies

To demonstrate the effectiveness of our hierarchy-aware cross-dataset loss suppression (HCLS), we compare a number of hierarchical loss strategies in Table 7 and Table 8.

- *Baseline* denotes that we do not take semantic hierarchy into account where each annotated bounding box has only one positive class label, and accordingly, we apply no loss adaptation.
- *Naive loss suppression* denotes that when calculating the classification loss, we ignore the losses over the children and parents for each category according to the semantic hierarchy of OID. This loss weighting incorporates semantic hierarchy by eliminating the effect of relationships between parents and children but also loses many positive samples for the superclasses from OID, resulting in inferior performance on OID.
- *Unified hierarchy* considers all parent-child relationships across datasets, according to the cross-dataset label duplication in Table 1, the cross-dataset semantic hierarchy in Table 2, and the original semantic hierarchy of OID for each category in unified label space. *Unified hierarchy*

Loss Strategy	COCO	MVD	OID
Baseline	44.1	<u>17.2</u>	65.3
Naive loss suppression	44.3	17.8	66.2
Unified hierarchy	43.1	17.1	67.1
OID hierarchy	43.5	16.2	67.6
+ HCLS	<u>44.2</u>	<u>17.2</u>	68.0

Table 8 Comparison on loss strategies. The used object detector is Cascade R-CNN based on SEER-RegNet32gf with NAS-FPN and Cascade RPN. The five models are trained for 420k iterations, with a base learning rate 0.01 which is decayed by a factor of 0.1 at 280k iterations. Note that the metric of COCO and MVD is mAP and the metric of OID is AP50. The best and the second best results are highlighted in **bold font** and under line, respectively.

sets all its parents as well as its semantic equivalent as positive and ignores the losses over all the child categories. This loss adaption enriches the training set for the superclasses with a lot of positive samples, which lead to a considerable performance gain on OID (+3.1 AP50 in Table 7 and +1.8 AP50 in Table 8).

But *Unified hierarchy* degrades the performance of COCO and MVD slightly. One possible reason is that although two categories from different datasets exactly match on the basis of language cues, they may be semantically different. For example, the *bear* from COCO represents a wide range of carnivorous mammals of the family Ursidae, such as brown bears, black bears, polar bears, and so on. However, its equivalent *bear* (/m/01dws) from OID includes these conventional bears and *teddy bears* (/m/0kmg4). So we had better not treat OID’s *bear* and its subclasses as positive samples for COCO’s *bear* because of this taxonomy inconsistency. We did observe a severe performance decline on COCO class *bear*: the AP of *bear* is 41.5 by using *Unified hierarchy*, while in the other four cases in Table 7, the AP of *bear* is over 65.1, and the best AP is 67.9 achieved by our HCLS.

- *OID hierarchy* is similar to *Unified hierarchy*, but only considering the semantic hierarchy of OID. *OID hierarchy* is a common practice for dealing with OID (X. Zhou et al., 2022), which does not incorporate the potential cross-dataset semantic hierarchy.
- Our loss strategy is denoted as *OID hierarchy* + *HCLS*, fully considering the semantic hierarchy

Dataset	Backbone	Strategy	mAP	AP50	epochs	Time	Memory
COCO	SEER-RegNet32gf	finetune	50.7	68.8	45	167	16
		freeze	50.9 (+0.2)	69.2 (+0.4)	72	160	10 (-6)
		finetune	49.9	68.3	64	238	16
		freeze	51.4 (+1.5)	69.8 (+1.5)	108	240	10 (-6)
	SEER-RegNet32gf	finetune	23.9	37.7	48	30	16
		freeze	24.1 (+0.2)	38.0 (+0.3)	80	30	10 (-6)
MVD	SEER-RegNet32gf	finetune	24.4	38.2	100	61	16
		freeze	24.8 (+0.4)	39.1 (+0.9)	160	60	10 (-6)
	SEER-RegNet256gf	finetune	25.8	40.4	60	70	60
		freeze	26.0 (+0.2)	40.9 (+0.5)	120	72	15 (-45)

Table 9 The object detectors are Cascade R-CNN enhanced with NAS-FPN ($\times 7$) and Cascade RPN. The training time is measured in hours and the GPU memory consumption is measured in GB / image. The models are trained with a batch size of 16 on 16 NVIDIA 3090 / A100 GPUs. For comparison purpose, we convert the training time on different devices to the training time on 8 NVIDIA 3090 GPUs uniformly.

of OID, label duplication, and semantic hierarchy among three datasets simultaneously. This loss adaption approach achieves the best AP on OID (+3.5 AP50 in Table 7 and +2.7 AP50 in Table 8), a slight improvement on COCO, and almost the same accuracy on MVD compared with *Baseline*.

4.5.3 Training Strategies

Table 9 compares two training strategies, *i.e.*, finetuning the overall object detector including the backbone (denoted as *finetune*), and the training strategy used in this paper, namely freezing the backbone during the training procedure (denoted as *freeze*). We evaluate the two strategies by training the models simultaneously on COCO or MVD, based on the lighter SEER backbone or the larger one, in terms of performance and GPU memory consumption.

- Performance

Based on the same detector configuration, *freeze* makes a consistent improvement in performance across datasets. With a longer training schedule, the benefit of *freeze* becomes even more striking. Especially on COCO, *finetune* reports a deterioration in performance with a longer learning schedule. A possible reason is that the backbone representations have drifted further away from the SEER original visual representations by the long training. The new representations

over-fitted on the relatively smaller downstream dataset probably weaken the object detector on COCO.

- GPU memory consumption

freeze needs much less GPU memory than *finetune* during the training procedure. We observe that *freeze* costs 10 GB of memory per image for the SEER-RegNet32gf-based model and 15 GB for the SEER-RegNet256gf-based model. However, *finetune* requires about 16 GB of memory per image for the SEER-RegNet32gf-based model and 60 GB for the SEER-RegNet256gf-based one. Consequently, it is easier to *freeze* to deploy model training with memory-limited computational resources, such as NVIDIA 3090.

4.5.4 Scaling Up and Finetuning

Scaling up during the inference procedure

As specified in Section 4.3, the short edges of the MVD images are resized to 2048 during the inference procedure to generate a better detection result because of plenty of tiny objects against the high resolution. The inference scaling up increases mAP by about 3 points on MVD in our RVC submission and significantly benefits the models in this paper as well. As shown in Fig. 4, the models obtained by the universal object detection training achieve the best performance when the short edge of the testing images is resized to 1600 (for Large-UniDet[S]) or 1400 (for Large-UniDet[L]).

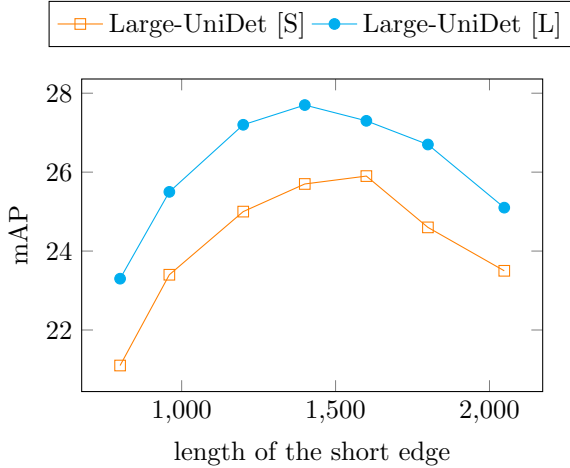


Fig. 4 The performance on MVD *vs.* the lengths of the short edge of the testing images. We obtain the best mAP at 25.9 with the 1600-pixel resized short edge based on the lighter backbone (Large-UniDet [S]), and obtain best mAP at 27.7 with the 1400-pixel resized short edge based on the larger one (Large-UniDet [L]). The initial mAP and highest mAP of both two models are reported in Table 10.

The 800-pixel short-edge baselines and the best results can be found in Table 10. Scaling up brings an impressive gain on MVD for the small and large models (+4.8 mAP and +4.4 mAP, respectively).

It is worth noting that we do not observe any improvement on COCO or OID when scaling up the size of the testing images since the inference scaling up improves the performance for small objects indeed but degrades that for the large, as stated in recent literature (Gao, Yu, Li, Morariu, & Davis, 2018). Given this, we believe that adapting the object detector to high-resolution images will benefit the detection of large objects and still maintain the improvement for the small ones.

Dataset-specific finetuning with scaling up

As an acceleration practice, training with high-resolution images following the low-resolution pre-training could produce satisfactory performance without too much computational cost during the training procedure (Singh & Davis, 2018). Following the universal object detection training, we conduct dataset-specific individual finetuning in higher resolution in joint consideration of the performance, training cost, and significant difference among the three datasets.

We use the cosine learning rate annealing with warm restarts (Loshchilov & Hutter, 2016) during the finetuning procedure. Without any alterations

Model	SU	FT	COCO	MVD	OID
[S]			48.8	21.1	68.5
	✓		-	25.9	-
	✓	✓	52.0	32.0	69.2
[L]			51.9	23.3	69.8
	✓		-	27.7	-
	✓	✓	53.5	33.2	70.5

Table 10 Comparison on the baseline, scaling up during the inference procedure (denoted as **SU**), and finetuning with higher-resolution training images (denoted as **FT**). The baseline is the universal object detection training without either scaling up the input size when testing or the following dataset-specific high-resolution finetuning. In the table, [S] and [L] represent Large-UniDet [S] and Large-UniDet [L], respectively. The metric of COCO and MVD is mAP and the metric of OID is AP50.

to the model design, the finetuning and inference configurations are specified that,

- for COCO, the model is trained for 24 epochs with six cyclical restarts where training images are scaled in a range of [640, 1200] and is evaluated with the 800-pixel resized short edge of testing images;
- for MVD, the model is trained for 24 epochs with six cyclical restarts where training images are scaled in a range of [1024, 2048] and is evaluated with the 2048-pixel resized short edge of testing images;
- for OID, the model is trained for 6 epochs with two cyclical restarts where training images are scaled in a range of [640, 1200] and is evaluated with the 800-pixel resized short edge of testing images.

Table 10 summarizes the results of the finetuning. Based on the lighter backbone, the dataset-specific high-resolution finetuning increases the performance by 3.2 mAP on COCO, 10.9 mAP on MVD, and 0.7 mAP on OID. While based on the larger backbone, the finetuning still retains considerable improvement on three datasets (+1.6 mAP on COCO, +9.9 mAP on MVD, and +0.7 mAP on OID, respectively).

4.6 Visualization

Figs. 5, 6 and 7 illustrate several qualitative results on COCO, MVD, and OID, respectively. The visualized predictions are generated by Large-UniDet

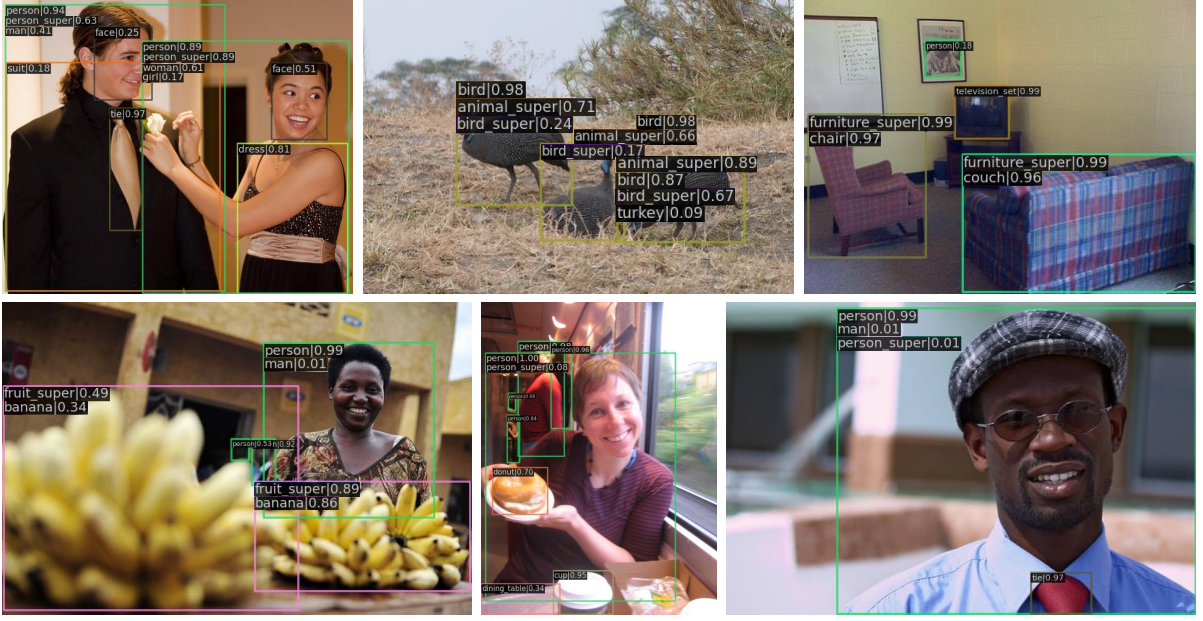


Fig. 5 Qualitative results on COCO *val* set. On the top left corner of each visualized bounding box, the predicted categories of which the corresponding confidence scores are greater than 0.01 are listed in the descending order of the confidence scores. The entry *classname_super* indicates this class is a superclass named *classname* in the unified label space.

based on SEER-RegNet256gf without conducting the following high-resolution dataset-specific individual finetuning described in Section 4.5.4. Since the multi-label classifiers are used in the detection heads of the universal object detector, we display up to five recognized categories for each bounding box with a confidence threshold. The multi-label box classification results disclose the nature of the category label duplication and semantic hierarchy across datasets in universal object detection. We will give an instance to go into details as follows.

In the upper-left visualization result in Fig. 5, we observe that the majority of categories, which are annotated in the original label space, and even some of the unannotated categories are detected successfully. The detected categories *man*, *woman*, *girl*, *person_super*, *face*, *suit*, *dress* are not included in the original label space of COCO but are still transferred from the other two datasets.

Label duplication. The categories *person* and *person_super* are semantically duplicated, resulting in the high confidence scores for the two people appearing in this image. To be specific, the man is classified as *person* with a confidence score of 0.94 and *person_super* with a confidence score of 0.63, meanwhile, the woman is classified as both *person* and *person_super* with a confidence score of 0.89.

Semantic hierarchy. As the categories *woman*, *man*, *girl*, *boy* are subclasses of *person*, the two people in this image are classified as one or more categories among these four subclasses.

Limitations More often, it is hard for the universal object detector to accurately detect or classify those unannotated categories in the unified label space by reason of the annotation inconsistency across the three datasets. For instance, the categories *eye*, *nose*, *mouth*, *hand* from OID are missed in the COCO visualized results in Fig. 5. Besides, the categories *person_super*, *man*, *woman*, *turkey*, which semantically match with the objects in the COCO images are of low confidence scores or failed to be detected in Fig. 5. A quite number of similar results on MVD or OID are illustrated in Fig. 6 and 7. The categories from other datasets are omitted in some cases.

Given the observation, we conjecture that our universal object detector partially overfits the distinctive characteristics of data domains. It seems that the model has found a way to cheat in universal object detection by remembering something unique to distinguish the testing images from different datasets, which might bring some harm to practical applications.



Fig. 6 Qualitative results on MVD *val* set. On the top left corner of each visualized bounding box, the predicted categories of which the corresponding confidence scores are greater than 0.1 are listed in the descending order of the confidence scores. The entry *classname_super* indicates this class is a superclass named *classname* in the unified label space.

Discussion This brings an interesting question, will unifying the annotations in the unified label space contribute to the universal object detectors in the individual performance on each dataset? As stated in the literature (Zhao et al., 2020), complementing the annotations for the unannotated objects by pseudo-labeling has been proven effective in the mixed unified full-annotated evaluation setting. However, the impact of annotation inconsistency on the individual datasets is not thoroughly investigated. As an initial exploration, in Section 4.5.2, we test a comparable label handling strategy, *Unified hierarchy*, to unify the annotations for those duplicated categories in semantics. But we do not observe any improvement on COCO or MVD in Tables 7 and 8. Despite that, we would leave the exhaustive study on this open question in future work.

5 Conclusion

Aiming at the million-scale multi-domain universal object detection problem, we propose several resource-efficient practices to employ large vision models for the robust visual representations across diverse datasets. Specifically, we freeze the parameters of large vision models and incorporate three important detector components with high capacity in our universal object detector. To deal with the cross-dataset label duplication and semantic hierarchy problems, we apply hierarchical taxonomy completion as well as a loss adaption strategy named hierarchy-aware cross-dataset loss suppression (HCLS) in the unified label space for multiple datasets. As an attempt for universal object detection, we hope our practices and findings can make

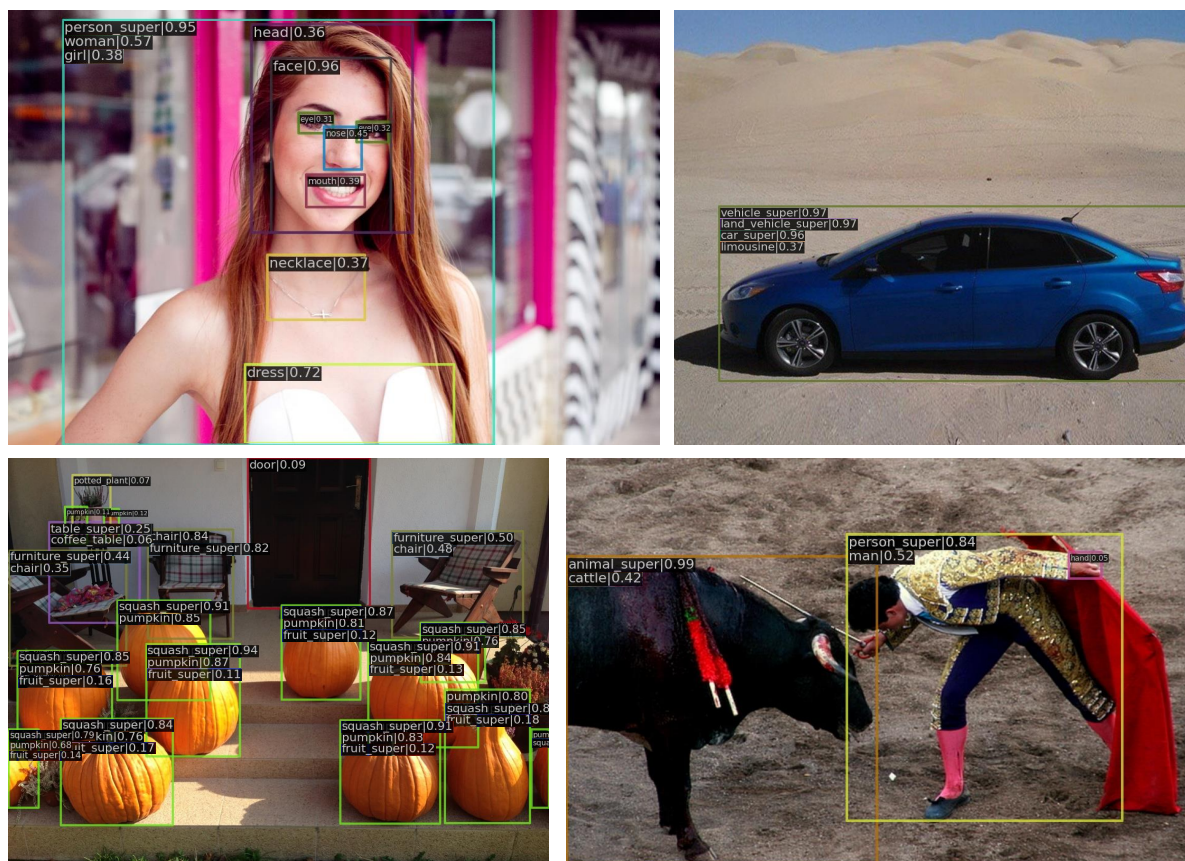


Fig. 7 Qualitative results on OID *val* set. On the top left corner of each visualized bounding box, the predicted categories of which the corresponding confidence scores are greater than 0.05 are listed in the descending order of the confidence scores. The entry *classname_super* indicates this class is a superclass named *classname* in the unified label space.

some contributions to real-world computer vision applications.

Data Availability Statement

The authors confirm the data supporting the findings of this work are available within the article or its supplementary materials.

References

- Azizi, S., Mustafa, B., Ryan, F., Beaver, Z., Freyberg, J., Deaton, J., ... others (2021). Big self-supervised models advance medical image classification. *Proceedings of the IEEE/CVF international conference on computer vision* (pp. 3478–3488).
- Bello, I., Fedus, W., Du, X., Cubuk, E.D., Srinivas, A., Lin, T.-Y., ... Zoph, B. (2021). Revisiting resnets: Improved training and scaling strategies. *Advances in Neural Information Processing Systems*, 34, 22614–22627.
- Bevandić, P., & Šegvić, S. (2022). Automatic universal taxonomies for multi-domain semantic segmentation. *arXiv preprint arXiv:2207.08445*.
- Bodla, N., Singh, B., Chellappa, R., Davis, L.S. (2017). Soft-nms—improving object detection with one line of code. *Proceedings of the IEEE international conference on computer vision* (pp. 5561–5569).

- Bu, X., Peng, J., Yan, J., Tan, T., Zhang, Z. (2021). Gaia: A transfer learning system of object detection that fits your needs. *Proceedings of the ieee/cvf conference on computer vision and pattern recognition* (pp. 274–283).
- Cai, L., Zhang, Z., Zhu, Y., Zhang, L., Li, M., Xue, X. (2022). Bigdetection: A large-scale benchmark for improved object detector pre-training. *Proceedings of the ieee/cvf conference on computer vision and pattern recognition* (pp. 4777–4787).
- Cai, Z., & Vasconcelos, N. (2018). Cascade r-cnn: Delving into high quality object detection. *Proceedings of the ieee conference on computer vision and pattern recognition* (pp. 6154–6162).
- Carion, N., Massa, F., Synnaeve, G., Usunier, N., Kirillov, A., Zagoruyko, S. (2020). End-to-end object detection with transformers. *European conference on computer vision* (pp. 213–229).
- Caron, M., Misra, I., Mairal, J., Goyal, P., Bojanowski, P., Joulin, A. (2020). Unsupervised learning of visual features by contrasting cluster assignments. *Advances in Neural Information Processing Systems*, 33, 9912–9924.
- Chen, K., Wang, J., Pang, J., Cao, Y., Xiong, Y., Li, X., ... others (2019). Mmdetection: Open mmlab detection toolbox and benchmark. *arXiv preprint arXiv:1906.07155*.
- Dai, Z., Liu, H., Le, Q.V., Tan, M. (2021). Coatnet: Marrying convolution and attention for all data sizes. *Advances in Neural Information Processing Systems*, 34, 3965–3977.
- Deng, J., Dong, W., Socher, R., Li, L.-J., Li, K., Fei-Fei, L. (2009). Imagenet: A large-scale hierarchical image database. *2009 ieee conference on computer vision and pattern recognition* (pp. 248–255).
- Devlin, J., Chang, M.-W., Lee, K., Toutanova, K. (2018). Bert: Pre-training of deep bidirectional transformers for language understanding. *arXiv preprint arXiv:1810.04805*.
- Dollar, P., Wojek, C., Schiele, B., Perona, P. (2011). Pedestrian detection: An evaluation of the state of the art. *IEEE transactions on pattern analysis and machine intelligence*, 34(4), 743–761.
- Gao, M., Yu, R., Li, A., Morariu, V.I., Davis, L.S. (2018). Dynamic zoom-in network for fast object detection in large images. *Proceedings of the ieee conference on computer vision and pattern recognition* (pp. 6926–6935).
- Ghiasi, G., Lin, T.-Y., Le, Q.V. (2019). Nas-fpn: Learning scalable feature pyramid architecture for object detection. *Proceedings of the ieee/cvf conference on computer vision and pattern recognition* (pp. 7036–7045).
- Gong, R., Dai, D., Chen, Y., Li, W., Van Gool, L. (2021). mdaLu: Multi-source domain adaptation and label unification with partial datasets. *Proceedings of the ieee/cvf international conference on computer vision* (pp. 8876–8885).
- Goyal, P., Duval, Q., Seessel, I., Caron, M., Singh, M., Misra, I., ... Bojanowski, P. (2022). Vision models are more robust and fair when pretrained on uncuration images without supervision. *arXiv preprint arXiv:2202.08360*.
- Gupta, A., Dollar, P., Girshick, R. (2019). Lvis: A dataset for large vocabulary instance segmentation. *Proceedings of the ieee/cvf conference on computer vision and pattern recognition* (pp. 5356–5364).
- Hasan, I., Liao, S., Li, J., Akram, S.U., Shao, L. (2021). Generalizable pedestrian detection: The elephant in the room. *Proceedings of the ieee/cvf conference on computer vision and pattern recognition* (pp. 11328–11337).

- He, K., Chen, X., Xie, S., Li, Y., Dollár, P., Girshick, R. (2022). Masked autoencoders are scalable vision learners. *Proceedings of the ieee/cvf conference on computer vision and pattern recognition* (pp. 16000–16009).
- He, K., Fan, H., Wu, Y., Xie, S., Girshick, R. (2020). Momentum contrast for unsupervised visual representation learning. *Proceedings of the ieee/cvf conference on computer vision and pattern recognition* (pp. 9729–9738).
- He, Y., Huang, G., Chen, S., Teng, J., Wang, K., Yin, Z., ... Shao, J. (2022). X-learner: Learning cross sources and tasks for universal visual representation. *European conference on computer vision* (pp. 509–528).
- Huang, J., Rathod, V., Sun, C., Zhu, M., Korattikara, A., Fathi, A., ... others (2017). Speed/accuracy trade-offs for modern convolutional object detectors. *Proceedings of the ieee conference on computer vision and pattern recognition* (pp. 7310–7311).
- Jia, C., Yang, Y., Xia, Y., Chen, Y.-T., Parekh, Z., Pham, H., ... Duerig, T. (2021). Scaling up visual and vision-language representation learning with noisy text supervision. *International conference on machine learning* (pp. 4904–4916).
- Joulin, A., Maaten, L.v.d., Jabri, A., Vasilache, N. (2016). Learning visual features from large weakly supervised data. *European conference on computer vision* (pp. 67–84).
- Kolesnikov, A., Zhai, X., Beyer, L. (2019). Revisiting self-supervised visual representation learning. *Proceedings of the ieee/cvf conference on computer vision and pattern recognition* (pp. 1920–1929).
- Kornblith, S., Shlens, J., Le, Q.V. (2019). Do better imagenet models transfer better? *Proceedings of the ieee/cvf conference on computer vision and pattern recognition* (pp. 2661–2671).
- Krishna, R., Zhu, Y., Groth, O., Johnson, J., Hata, K., Kravitz, J., ... others (2017). Visual genome: Connecting language and vision using crowdsourced dense image annotations. *International journal of computer vision*, 123(1), 32–73.
- Kuznetsova, A., Rom, H., Alldrin, N., Uijlings, J., Krasin, I., Pont-Tuset, J., ... others (2020). The open images dataset v4. *International Journal of Computer Vision*, 128(7), 1956–1981.
- Lambert, J., Liu, Z., Sener, O., Hays, J., Koltun, V. (2020). Mseg: A composite dataset for multi-domain semantic segmentation. *Proceedings of the ieee/cvf conference on computer vision and pattern recognition* (pp. 2879–2888).
- Lin, F., Xu, H., Li, H., Xiong, H., Qi, G.-J. (2021). Auto-encoding transformations in reparameterized lie groups for unsupervised learning. *Proceedings of the aaai conference on artificial intelligence* (Vol. 35, pp. 8610–8617).
- Lin, T.-Y., Dollár, P., Girshick, R., He, K., Hariharan, B., Belongie, S. (2017). Feature pyramid networks for object detection. *Proceedings of the ieee conference on computer vision and pattern recognition* (pp. 2117–2125).
- Lin, T.-Y., Maire, M., Belongie, S., Hays, J., Perona, P., Ramanan, D., ... Zitnick, C.L. (2014). Microsoft coco: Common objects in context. *European conference on computer vision* (pp. 740–755).
- Liu, S., Qi, L., Qin, H., Shi, J., Jia, J. (2018). Path aggregation network for instance segmentation. *Proceedings of the ieee conference on computer vision and pattern recognition* (pp. 8759–8768).
- Liu, Y., Wang, Y., Wang, S., Liang, T., Zhao, Q., Tang, Z., Ling, H. (2020). Cbnet: A novel composite backbone network architecture for object detection. *Proceedings of*

- the aaai conference on artificial intelligence* (Vol. 34, pp. 11653–11660).
- Liu, Z., Hu, H., Lin, Y., Yao, Z., Xie, Z., Wei, Y., ... others (2022). Swin transformer v2: Scaling up capacity and resolution. *Proceedings of the ieee/cvf conference on computer vision and pattern recognition* (pp. 12009–12019).
- Loshchilov, I., & Hutter, F. (2016). Sgdr: Stochastic gradient descent with warm restarts. *arXiv preprint arXiv:1608.03983*.
- Meng, L., Dai, X., Chen, Y., Zhang, P., Chen, D., Liu, M., ... Jiang, Y.-G. (2022). Detection hub: Unifying object detection datasets via query adaptation on language embedding. *arXiv preprint arXiv:2206.03484*.
- Micikevicius, P., Narang, S., Alben, J., Diamos, G., Elsen, E., Garcia, D., ... others (2018). Mixed precision training. *International conference on learning representations*.
- Neuhold, G., Ollmann, T., Rota Bulo, S., Kontschieder, P. (2017). The mapillary vistas dataset for semantic understanding of street scenes. *Proceedings of the ieee international conference on computer vision* (pp. 4990–4999).
- Pang, J., Chen, K., Shi, J., Feng, H., Ouyang, W., Lin, D. (2019). Libra r-cnn: Towards balanced learning for object detection. *Proceedings of the ieee/cvf conference on computer vision and pattern recognition* (pp. 821–830).
- Radford, A., Kim, J.W., Hallacy, C., Ramesh, A., Goh, G., Agarwal, S., ... others (2021). Learning transferable visual models from natural language supervision. *International conference on machine learning* (pp. 8748–8763).
- Radosavovic, I., Kosaraju, R.P., Girshick, R., He, K., Dollár, P. (2020). Designing network design spaces. *Proceedings of the ieee/cvf conference on computer vision and pattern recognition* (pp. 10428–10436).
- Ranftl, R., Lasinger, K., Hafner, D., Schindler, K., Koltun, V. (2020). Towards robust monocular depth estimation: Mixing datasets for zero-shot cross-dataset transfer. *IEEE transactions on pattern analysis and machine intelligence*.
- Ren, S., He, K., Girshick, R., Sun, J. (2015). Faster r-cnn: Towards real-time object detection with region proposal networks. *Advances in neural information processing systems*, 28.
- Shao, J., Chen, S., Li, Y., Wang, K., Yin, Z., He, Y., ... others (2021). Intern: A new learning paradigm towards general vision. *arXiv preprint arXiv:2111.08687*.
- Shao, S., Li, Z., Zhang, T., Peng, C., Yu, G., Zhang, X., ... Sun, J. (2019). Objects365: A large-scale, high-quality dataset for object detection. *Proceedings of the ieee/cvf international conference on computer vision* (pp. 8430–8439).
- Singh, B., & Davis, L.S. (2018). An analysis of scale invariance in object detection snip. *Proceedings of the ieee conference on computer vision and pattern recognition* (pp. 3578–3587).
- Sun, C., Shrivastava, A., Singh, S., Gupta, A. (2017). Revisiting unreasonable effectiveness of data in deep learning era. *Proceedings of the ieee international conference on computer vision* (pp. 843–852).
- Tan, M., Pang, R., Le, Q.V. (2020). Efficientdet: Scalable and efficient object detection. *Proceedings of the ieee/cvf conference on computer vision and pattern recognition* (pp. 10781–10790).
- Vasconcelos, C., Birodkar, V., Dumoulin, V. (2022). Proper reuse of image classification features improves object detection. *Proceedings of the ieee/cvf conference on computer vision and pattern recognition* (pp. 13628–13637).

- Vu, T., Jang, H., Pham, T.X., Yoo, C. (2019). Cascade rpn: Delving into high-quality region proposal network with adaptive convolution. *Advances in neural information processing systems*, 32.
- Wang, X., Cai, Z., Gao, D., Vasconcelos, N. (2019). Towards universal object detection by domain attention. *Proceedings of the ieee/cvf conference on computer vision and pattern recognition* (pp. 7289–7298).
- Xu, H., Fang, L., Liang, X., Kang, W., Li, Z. (2020). Universal-rcnn: Universal object detector via transferable graph r-cnn. *Proceedings of the aaai conference on artificial intelligence* (Vol. 34, pp. 12492–12499).
- Xu, H., Zhang, X., Li, H., Xie, L., Dai, W., Xiong, H., Tian, Q. (2022). Seed the views: Hierarchical semantic alignment for contrastive representation learning. *IEEE Transactions on Pattern Analysis and Machine Intelligence*.
- Yu, J., Jiang, Y., Wang, Z., Cao, Z., Huang, T. (2016). Unitbox: An advanced object detection network. *Proceedings of the 24th acm international conference on multimedia* (pp. 516–520).
- Yuan, L., Chen, D., Chen, Y.-L., Codella, N., Dai, X., Gao, J., ... others (2021). Florence: A new foundation model for computer vision. *arXiv preprint arXiv:2111.11432*.
- Zhang, S., Benenson, R., Schiele, B. (2017). Citypersons: A diverse dataset for pedestrian detection. *Proceedings of the ieee conference on computer vision and pattern recognition* (pp. 3213–3221).
- Zhao, X., Schuster, S., Sharma, G., Tsai, Y.-H., Chandraker, M., Wu, Y. (2020). Object detection with a unified label space from multiple datasets. *European conference on computer vision* (pp. 178–193).
- Zhou, B., Zhao, H., Puig, X., Fidler, S., Barriuso, A., Torralba, A. (2017). Scene parsing through ade20k dataset. *Proceedings of the ieee conference on computer vision and pattern recognition* (pp. 633–641).
- Zhou, X., Koltun, V., Krähenbühl, P. (2022). Simple multi-dataset detection. *Proceedings of the ieee/cvf conference on computer vision and pattern recognition* (pp. 7571–7580).